

**EFFECT OF CARBURISATION PROCESS ON  
THE WEAR OF STEEL**



**ROONIE PROTASIOUS**

**UMS**  
UNIVERSITI MALAYSIA SABAH

**FACULTY OF ENGINEERING  
UNIVERSITI MALAYSIA SABAH  
2016**

**EFFECT OF CARBURISATION PROCESS ON  
THE WEAR OF STEEL**

**ROONIE PROTASIUS**



**UMS**

**THESIS SUBMITTED IN FULFILLMENT FOR  
THE DEGREE OF MASTER OF ENGINEERING**

**FACULTY OF ENGINEERING  
UNIVERSITI MALAYSIA SABAH  
2016**

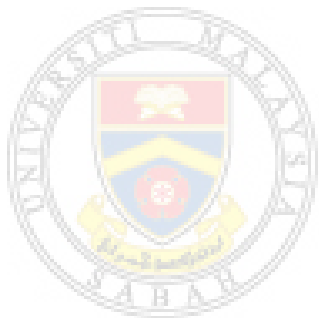
## **DECLARATION**

I hereby declare that the material in this thesis is my own except for quotations, excerpts, equations, summaries and references, which have been duly acknowledged.

05 February 2016

---

Ronie Protasius  
MK1311004T



**UMS**  
UNIVERSITI MALAYSIA SABAH

## CERTIFICATION

NAME : **ROONIE PROTASIUS**  
MATRIC NO. : **MK1311004T**  
TITLE : **EFFECT OF CARBURISATION PROCESS ON THE WEAR OF STEEL**  
DEGREE : **MASTER OF ENGINEERING (MECHANICAL ENGINEERING)**  
VIVA DATE : **06 NOVEMBER 2015**

### DECLARED BY

- 

**1. SUPERVISOR**  
Prof. Madya Dr. Willey Liew Yun Hsien      Signature

---
- 2. CO-SUPERVISOR**  
Dr. Noor Ajian Mohd Lair

---

## **ACKNOWLEDGEMENT**

I would like to take this opportunity to express my highest gratitude to my supervisor, Assoc. Prof. Dr Willey Liew Yun Hsien and co-supervisor, Dr Noor Ajian Mohd Lair for the excellent supervision, guidance, encouragement and financial support during my tenure of study in my Master by Research course. Their broad knowledge and wisdom have inspired me tremendously throughout the entire course.

I would also like to thank the staff in Fakulti Kejuruteraan (FKJ), UMS namely Mr Jasmi Jaya, Mr Alexander Kong, Mr Saiful Azwar, Mr Saiful Safiq, Mr. Abdullah Tarikin, Mr John Abdullah, Mr Munap Salleh, Mr Jester Ling, Mr Saffuan Baharin, Dr Nancy Siambun, Assoc. Prof. Dr Rachel Mansa and all the others which I did not mention here for the invaluable help, encouragement and guidance towards the completion of my course.

My special thanks to Politeknik Kota Kinabalu for the usage of their foundry and metallurgy lab for the carburisation process. I also wish to thank Jabatan Kerja Raya Malaysia (JKR) and Jabatan Perkhidmatan Awam Malaysia (JPA) for the opportunity given to me to further my study in Universiti Malaysia Sabah (UMS).

Finally, I would like to dedicate a special appreciation to my wife, daughter and family members for all the support that they have provided throughout the entire course.

## ABSTRACT

Electro-carburisation process based on liquid carburisation process had been carried out to investigate the effect of the carburization process on the resulting hardness, microstructure change, and the sliding wear resistance of mild steel under dry and lubrication conditions. The carburisation process was conducted in carbonate salts mixtures of  $\text{Na}_2\text{CO}_3\text{-NaCl}$ . The electro-carburisation process was first performed and followed by post-carburisation cleaning where subsequent analysis such as hardness test, metallographic observation, EDX/SEM and XRD were then carried out in order to investigate the effect of the carburisation process on the mild steel. Carburisation process resulted in a remarkable increase in the hardness leading to an enhancement of adhesive and abrasive wear resistance, as well as load carrying capacity. Increasing the duration of the carburisation process from 1 hour to 3 hours resulted in higher peak hardness (727 HV/795 HV), greater case depth (50-100 $\mu\text{m}$ /660 $\mu\text{m}$ ), higher amount of carbide in the grain boundaries and larger retained austenite grains. The surface of the carburised steel was dominated by retained austenite. Towards the core, the amount of retained austenite reduced while the amount of martensite increased. The austenite microstructure in the steel carburised for 1 hour exhibited higher cracking and fracture resistance as compared to the steel carburised for 3 hours. The low cracking and fracture resistance of the steel carburised for 3 hours could be due to its large grain size and high amount of cementite in the grain boundaries as the fatigue strength reduced with an increase in the grain size and the presence cementite could act as fatigue crack initiators. The superior wear resistance of the martensite, as compared to the austenite, could be attributed to its high cracking and adhesive wear resistance owing to its high hardness and tendency to form oxide. The friction was governed by the wear mechanism and the type of microstructure at the worn scar sliding on the carbide ball. It was found that surface fracture and sliding on martensite resulted in higher friction coefficient. The superior wear resistance and load carrying capacity of the carburised steel was also evident under oil lubrication condition. Compared to the austenite, the martensite showed higher tendency to react with the carbon in the oil under extreme boundary lubrication which in turn resulted in a significant drop in the friction coefficient after the running in process.

## **ABSTRAK**

### **EFFECT OF CARBURISATION PROCESS ON THE WEAR OF STEEL ( KESAN PROSES PENGKARBONAN KE ATAS KEHAUSAN KELULI )**

Proses 'electro-carburisation' berdasarkan proses pengkarbonan cecair telah dijalankan untuk mengkaji kesan daripada proses pengkarbonan pada kekerasan yang terhasil, perubahan mikrostruktur, dan rintangan haus gelongsor keluli lembut di bawah keadaan kering dan pelinciran. Proses pengkarbonan telah dijalankan dengan menggunakan campuran garam karbonat  $\text{Na}_2\text{CO}_3\text{-NaCl}$ . Proses 'elektro-carburisation' dilakukan terlebih dahulu diikuti dengan pembersihan ke atas spesimen yang telah menjalani proses pengkarbonan. Analisis berikutnya seperti ujian kekerasan, pemerhatian 'metallographic', EDX / SEM dan XRD kemudiannya dijalankan untuk menyiasat kesan proses pengkarbonan pada keluli karbon rendah. Proses pengkarbonan menyebabkan peningkatan kekerasan yang ketara yang membawa kepada peningkatan rintangan kehausan las dan perekat serta beban bawaan yang lebih tinggi. Meningkatkan masa proses pengkarbonan dari 1 jam hingga 3 jam menghasilkan kekerasan puncak yang lebih tinggi (727 HV / 795 HV), salutan yang lebih mendalam (50-100 $\mu\text{m}$  / 660 $\mu\text{m}$ ), jumlah karbida yang lebih tinggi di sempadan bijian dan bijirin austenit yang lebih besar. Permukaan keluli yang menjalani proses pengkarbonan dikuasai oleh austenit tersimpan. Ke arah teras, jumlah austenit tersimpan semakin berkurangan manakala jumlah martensit meningkat. Mikrostruktur austenit dalam keluli yang telah dikarbonkan selama 1 jam mempamerkan rintangan keretakan dan patah yang lebih tinggi berbanding dengan keluli yang telah dikarbonkan selama 3 jam. Rintangan keretakan dan patah yang rendah oleh keluli yang dikarbonkan untuk 3 jam berkemungkinan disebabkan oleh saiz butiran yang besar dan jumlah sementit yang tinggi di sempadan bijian menyebabkan kekuatan lesu berkurangan yang mana peningkatan dalam saiz butiran dan kehadiran sementit boleh bertindak sebagai pemula retak-lesu. Rintangan haus martensit yang lebih tinggi berbanding austenit boleh dikaitkan dengan rintangan keretakan dan perekat yang lebih tinggi disebabkan oleh kekerasan yang tinggi dan kecenderungan untuk membentuk oksida. Geseran telah dikawal oleh mekanisme kehausan dan jenis mikrostruktur yang terdapat di parut kehausan di mana bola karbida menggelongsor di atasnya. Didapati bahawa keretakan permukaan dan menggelongsor di atas martensit menyebabkan pekali geseran yang lebih tinggi. Kapasiti rintangan haus yang lebih tinggi dan beban bawaan keluli yang dikarbonkan juga dapat dilihat di bawah kehadiran minyak pelincir. Berbanding dengan austenit, martensit menunjukkan kecenderungan lebih tinggi untuk bertindak balas dengan karbon dalam minyak di bawah pelinciran sempadan melampau yang seterusnya mengakibatkan penurunan ketara dalam pekali geseran selepas berjalan dalam proses.

# TABLE OF CONTENTS

	Page
<b>TITLE</b>	i
<b>DECLARATION</b>	ii
<b>CERTIFICATION</b>	iii
<b>ACKNOWLEDGEMENT</b>	iv
<b>ABSTRACT</b>	v
<b>ABSTRAK</b>	vi
<b>TABLE OF CONTENTS</b>	vii
<b>LIST OF TABLES</b>	x
<b>LIST OF FIGURES</b>	xi
<b>LIST OF ABBREVIATIONS</b>	xxi
<b>LIST OF SYMBOLS</b>	xxii
<b>LIST OF EQUATIONS</b>	xxiii
<b>CHAPTER 1: INTRODUCTION</b>	1
1.1 Research background	1
1.2 Electro-carburisation process	4
1.3 The wear of carburised steel	5
1.4 Research objectives	6
1.5 Scope of thesis	6
<b>CHAPTER 2: LITERATURE REVIEW</b>	8
2.0 Introduction	8
2.1 Low carbon steel and its properties	8
2.1.1 Carburisation of low carbon steel	10
2.1.2 Carbon diffusion during carburisation	13
2.1.3 Quenching	17
2.1.4 Transformation product from carburisation process	21
2.1.5 Martensite	23
2.1.6 Bainite	27



2.1.7	Austenite / Retained austenite / ferrite	28
2.1.8	Pearlite	32
2.1.9	Cementite	33
2.2	Molten Salt Electro-Carburisation	35
2.2.1	Electrochemical reaction during the carburisation process	39
2.3	Case Depth and Hardness	41
2.4	Grain Size	45
2.5	Internal Oxidation	46
2.6	Decarburisation process	48
2.7	The effect of retained austenite on the wear behavior	50
2.8	Wear under sliding motion (reciprocating)	53
2.8.1	Contact Surface	57
2.8.2	Coefficient of friction	60
2.8.3	Wear Mechanism	66
2.8.4	Adhesive wear	66
2.8.5	Abrasive wear	69
2.8.6	Fatigue	72
2.8.7	Oxidative wear	74
2.9	Lubricant effect on the wear behavior of carburised product	77
2.9.1	Lubricant regime	78
2.9.2	Wear mechanism under lubricated sliding	80
2.9.3	Element change during the wear under lubricated sliding	80
2.10	Summary	81
<b>CHAPTER 3: EXPERIMENTAL PROCEDURE</b>		<b>83</b>
3.0	Introduction	83
3.1	Material selection and preparation	84
3.2	The Carburisation Process	85
3.2.1	Equipment set up	87
3.2.2	Carburisation parameters	89
3.3	Post preparation of carburised specimens	91
3.3.1	Sample cutting and surface polishing	92

3.4	Wear test	94
3.4.1	COF Measurement	96
3.4.2	Wear Measurement	96
3.5	Sample Analysis	97
3.5.1	Microindentation Hardness Test	98
3.5.2	Metallographic analysis	100
3.5.3	XRD	102
3.5.4	Profilemeter	105
3.5.5	SEM/EDS	106
3.6	Summary	109
<b>CHAPTER 4: RESULTS AND DISCUSSIONS</b>		110
4.0	Introduction	110
4.1	Voltage and current effect during carburisation process	110
4.2	Surface characteristic and microstructure	112
4.2.1	Hardness and surface roughness measurement	112
4.2.2	Surface characterization	114
4.3	Dry sliding test	124
4.3.1	Frictional forces and wear	124
4.4	Lubricated sliding test	139
4.4.1	Frictional forces and wear	139
<b>CHAPTER 5: CONCLUSION AND FUTURE WORK</b>		159
5.1	Conclusion	159
5.2	Future Work	160
<b>REFERENCES</b>		162

## LIST OF TABLES

	Page
Table 1.1: Engineering method of surface hardening of steels	2
Table 2.1: Example of chemical composition of low carbon steel	9
Table 2.2: Typical characteristic of diffusion treatment	11
Table 2.3 : Tabulation of error function value	14
Table 2.4: Activation energy for diffusing species	17
Table 2.5: An example of cooling rate for steel	21
Table 3.1: Chemical composition for the material used (in weight % ) as per mill certificate obtained	85
Table 3.2: The carburisation main parameters used by (a) Siambun (2011) and (b) this research	90
Table 3.3: The range of loads applied during the reciprocating test	96
Table 3.4: The characterised surface in this research	104
Table 4.1: Surface roughness of the test specimens	114
Table 4.2: Samples of the EDX results for (a) the martensite packets and (b) the retained austenite grains of the C3 specimen after sliding at 50N 20Hz	121
Table 4.3: Samples of the EDX results for (a) the martensite packets and (b) the retained austenite grains in the worn scar of the C3 specimen after sliding at 50N 20Hz	139
Table 4.4: The Stribeck value for different applied normal load	143

## LIST OF FIGURES

	Page
Figure 1.1: The electro-carburisation process set up.	3
Figure 1.2: The peak hardness obtained from the carburisation process.	5
Figure 2.1: Effect of carbon percentage on the maximum hardness of steel.	9
Figure 2.2: Carbon diffusion into the surface of the low carbon steel.	10
Figure 2.3: (a) Iron - Carbon phase diagram (b) The arrangement of atoms in Body Centered Cubic (BCC) and Face Centered Cubic (FCC).	12
Figure 2.4: (a) The non steady state type of diffusion and (b) Concentration of carbon atoms versus distance from the steel surface.	15
Figure 2.5: Carbon concentration as a function of temperature	16
Figure 2.6: (a) Typical Isothermal Transformation Diagram (b) Isothermal Transformation Diagram for 1008 steel.	19
Figure 2.7: (a) A correlation between IT and CCT for eutectoid steel (b) Moderately rapid and slow cooling curve superimposed on a CCT diagram for eutectoid steel.	20
Figure 2.8: Microstructures: (a), martensite; (b) martensite with a trace of very fine pearlite (dark); (c) martensite and very fine pearlite; (d) fine pearlite; (e) coarse pearlite. All etched with nital. X500 (f) Schematic diagram, illustrating the relation between the S-curve, continuous cooling curves, and resulting microstructures of eutectoid carbon steel.	23
Figure 2.9: The carbon content based on temperature which will affect the start of the martensite ( $M_s$ ) by substitution into equation 2.3.	24

Figure 2.10:	(a) Steel hardness for various carbon contents and percentages of martensite for some low-alloy steels (b) Hardness of martensitic microstructures as a function of steel carbon content.	25
Figure 2.11:	(a) Microstructure of lath martensite in iron containing 0.18wt.%C (b) Microstructure of plate martensite in iron containing 1.86wt.%C.	26
Figure 2.12:	(a) Microstructure of bainite (b) Isothermal transformation diagram for eutectoid composition.	28
Figure 2.13:	Microstructure of (a) ferrite (b) Austenite (c ) Mixture of microstructures under SEM.	29
Figure 2.14:	Microstructure of the carburised specimens cooled naturally in air using cell voltage of (a) 1.0V (b) 1.5V.	30
Figure 2.15:	Microstructure of retained austenite.	30
Figure 2.16:	(a) CCT diagram with related hardness and (b) percentage of microstructural constituents for a 20Ni-Mo-6Cr steel carburised at 930°C for 30 min.	31
Figure 2.17:	Influence of carbon content on retained austenite content	32
Figure 2.18:	The photomicrograph of 0.38 wt.%C steel which contain microstructure of pearlite and proeutectoid ferrite.	33
Figure 2.19:	(a) A micrograph showing direct quenched carburised steel having grain boundary carbide (b) Massive carbides (c) Film carbides.	34
Figure 2.20:	Three types of carbides (a) Massive carbides (b) Film carbides (c) intergranular carbides.	35
Figure 2.21:	Electrolytic case hardening basic apparatus.	36
Figure 2.22:	The carbon gradient produced by liquid carburisation at different temperature.	37
Figure 2.23:	The basic equipment set up for the developed carburisation process.	38
Figure 2.24:	The NaCl-Na <sub>2</sub> CO <sub>3</sub> melting temperature.	41

Figure 2.25:	(a) Effective case depth as a function of time and (b) Effect of carbon on the hardness of various microstructures observed in plain carbon steel.	43
Figure 2.26:	(a) Effect of mol ratio and (b) voltage on the case depth of carburised steel.	44
Figure 2.27:	The grain size measurement based on ASTM E112-12; (a) ASTM 6, (b)ASTM7 (c) ASTM8, (d)ASTM9.	46
Figure 2.28:	Internal oxidation in carburised steel .	47
Figure 2.29:	Oxidation potential of various alloying element in iron.	48
Figure 2.30:	Equilibrium pressure of CO and CO <sub>2</sub> for 2CO → CO <sub>2</sub> + C reaction.	49
Figure 2.31:	The effect of decarburisation on carburised steel where a) showed severe carburisation effect, b) slight carburisation and c) no decarburisation occur.	50
Figure 2.32:	Amount of retained austenite for direct quenched SAE 8620 steel.	51
Figure 2.33:	Retained austenite (white) and martensite in the surfaces of carburised steel (a) 40% and (b) 15%.	52
Figure 2.34:	Relative wear resistance as a function of hardness.	53
Figure 2.35:	(a)single cycle (b) and repeated cycle wear.	54
Figure 2.36:	General model of surface fatigue failure. Stage I, stress cycling on the surface; stage II, nucleation of cracks in the near-surface region; stage III, Crack growth; Stage IV, crack propagate; Stage V, crack intersection with the surface; Stage VI, formation of looseparticles.	55
Figure 2.37:	Micrograph of wear under repeated cycle.	56
Figure 2.38:	A classification of mechanical wear processes.	57
Figure 2.39:	An illustration of a two surfaces asperities in contact.	58
Figure 2.40:	Measurement of surface roughness.	59
Figure 2.41:	Typical surface finish for basic machining process.	59
Figure 2.42:	Basic definition of coefficient of friction COF.	61

Figure 2.43:	The effect of normal load on the COF where (a) constant value COF, (b) increasing COF and (c) decreasing COF.	62
Figure 2.44:	COF as a function of sliding distance with (a) a typical S-shaped curve showing run-in period (b) four hypothetical case.	64
Figure 2.45:	Polycrystalline copper slider across grain boundary on copper bicrystal (a) from 210 to 111 and (b) 110 to 210.	65
Figure 2.46:	(a) Adhesive wear reaction (b) A micrograph showing a surface subjected to adhesive wear.	67
Figure 2.47:	(a) Fretting wear which occur due to small oscillation(b) Enlarged micrograph of the wear area.	68
Figure 2.48:	Scuffing limit of non treated stainless steel.	68
Figure 2.49:	Galling wear mechanism.	69
Figure 2.50:	SEM images of the abrasive wear mechanism produced by (a) plowing, (b) wedge formation and (c) cutting.	70
Figure 2.51:	(a) Abrasive wear by two body and three body (b) A micrograph of a surface subjected to abrasion.	71
Figure 2.52:	Schematic drawing of two body abrasive wear resistance of different materials measured in the pin abrasion test as a function of their bulk hardness.	72
Figure 2.53:	Strain level in deformed surface.	73
Figure 2.54:	Model for fatigue wear.	74
Figure 2.55:	Model for oxidative wear.	75
Figure 2.56:	Examples of sliding wear surfaces after the formation of oxide layer.	76
Figure 2.57:	Stribeck curve showing the lubrication regimes.	79
Figure 2.58:	The lubrication regimes associated with the fluid film thicknesswhere (a) hydrodynamic, (b) Elastohydrodynamic, (c) Mixed and (d) boundary region.	79
Figure 2.59:	Depth profile by Auger electron spectroscopy of gray cast iron. (a) initial state , (b) worn state.	81
Figure 3.1:	Flow diagram of the overall experimental procedure.	84

Figure 3.2:	The specimen holder for reciprocating test.	85
Figure 3.3:	The equipment set up for the production of carburised specimens.	86
Figure 3.4:	(a) Retort and Lid (b) Tightening of the lid to the retort by clamps.	88
Figure 3.5:	(a) The interconnection to the thermometer and drescher bottle and (b) The setup for the whole equipment .	88
Figure 3.6:	(a) Quenching of the carburised specimens in water (b) Thecarburised specimens.	89
Figure 3.7:	(a) The location of the samples for the hardness test and (b)the sectioned sample.	91
Figure 3.8:	Figure 3.8 : Ultrasonic cleaner.	92
Figure 3.9:	(a) Cutter and (b) Leco Spectrum System 2000 surface polish(c) The specimen in resin mould.	93
Figure 3.10:	(a) The specimen and ball holder with the specimen loaded(b) The reciprocating station.	95
Figure 3.11:	The reciprocating test based on ASTM G133.	95
Figure 3.12:	a) Mitutoyo Vickers micro hardness tester and b) diamond shaped indenter.	99
Figure 3.13:	Illustration of the diamond indenter.	100
Figure 3.14:	(a) Optical microscope coupled with (b) Digital camera	101
Figure 3.15:	The polishing pass for the metallographic analysis for different layer.	101
Figure 3.16:	Bragg's Law schematic diagram for X-ray reflection on the crystal atomic plane.	103
Figure 3.17:	The XRD equipment used in the research.	104
Figure 3.18:	(a) Tokyo Seimetsu profilemeter (b) Stylus tip.	106
Figure 3.19:	Electron beam interaction diagram.	106
Figure 3.20:	Sample of EDX reading.	107
Figure 3.21:	(a)The SEM (b) EDS used in the research.	108
Figure 4.1:	I-V graphs for the carburization where (a) 3 hours (b) 1 hour.	111



Figure 4.2:	Variation of the subsurface hardness of the carburised steel specimens carburised. The hardness value at distance = 0 $\mu\text{m}$ is the hardness of the surface.	113
Figure 4.3:	Optical micrographs of the cross-section of the (a) C1 and (b) C3 specimens where CD marked the total case depth of the C1 and C3 specimens.	113
Figure 4.4:	The microstructure of the C1 specimen at the (a) surface after slight polishing (b) subsurface 5 $\mu\text{m}$ beneath the surface (c) subsurface 10 $\mu\text{m}$ beneath the surface (d) subsurface 20 $\mu\text{m}$ beneath the surface, (e) and (f) subsurface 100 $\mu\text{m}$ beneath the surface.	115
Figure 4.5:	XRD analysis on the surface and sub-surface of the C1 specimen.	119
Figure 4.6:	SEM images of the surfaces of the (a-b) C1 and (c-d) C3 specimens. C1 specimen had grains with a diameter of 10-20 $\mu\text{m}$ . C3 specimen had larger grains with a diameter of 10-150 $\mu\text{m}$ and greater amount of network elements rich in carbon in the grain boundaries.	120
Figure 4.7:	EDX analysis of the retained austenite grains in the C3 specimen.	122
Figure 4.8:	EDX analysis of the network element in the grain boundaries of the C3 specimen.	122
Figure 4.9:	The microstructure of the C3 specimen at the (a) surface after slight polishing and (b) subsurface 5 $\mu\text{m}$ beneath the surface. Numerous amount of carbide appeared in the grain boundaries of the retained austenite and the martensite.	123
Figure 4.10:	Examination of the core of the carburised mild steel using an optical microscope showed that it had ferrite, retained austenite and martensite.	123
Figure 4.11:	Variation of the coefficient of friction in sliding steel carburised for 3 hours at 10N 2Hz and 10N 20Hz.	124

Figure 4.12:	Effect of load on the average steady-state coefficient of friction (COF) at (a) 2 Hz and (b) 20 Hz. The average steady-state COF was computed based on the last 20 minutes of steady-state sliding as illustrated in figure 4.11.	125
Figure 4.13:	The wear depth for the C3 specimen under test parameter of 10N2Hz.	126
Figure 4.14:	Effect of load on the volume loss at (a) 2 Hz and (b) 20 Hz.	127
Figure 4.15:	SEM images of the (a) NC steel after sliding at 10N 2Hz (b) NC steel after sliding at 150N 20Hz, and (c) M3 steel after sliding at 400N 2Hz.	128
Figure 4.16:	Profiles of the worn scars of (a) M1 specimens after sliding at 50N 2Hz, (b) M1 specimens after sliding at 400N 2Hz and (c) C1 specimens after sliding at 50N 2Hz.	129
Figure 4.17:	Overview of the worn scars of the C3 specimens after sliding at (a) 10N 2Hz (b) 50N 2Hz (c) 150 N 2Hz (d) 10N 20Hz (e) 50N 20Hz and (f) 150N 20Hz. At 50N 2Hz and 10N 20Hz, cracking and fracture occurred on the entire worn scars dominated by austenite. At 50N 20Hz, cracking and fracture took place merely on the side of the worn scar dominated by austenite.	132
Figure 4.18:	SEM images of the cracks and fracture on the worn scar of the C3 specimen after sliding at 50N 2Hz taken at (a) 1600 x and (b) 3000 x magnification. MP: Martensite packet. A: Austenite. F:Fracture. (c) Cracks and (b) work materials on the worn scar of the C1 specimens after sliding at 50N 2Hz.	133
Figure 4.19:	SEM of the wear debris obtained in sliding (a) M1 and (b) C1 specimens at 50N 20Hz.	135
Figure 4.20:	EDX-element-mappings of O element at the side and centre of the C3 specimen after sliding at 50N 20Hz.	136

Figure 4.21:	EDX-element-mappings of O, Fe, C and W elements at the side of the worn scar of the C3 specimen after sliding at 50N 20Hz. Martensite packets had higher concentration of O element as compared to the austenite region. MP: Martensite packet. A: Austenite.	137
Figure 4.22:	EDX-element-mappings of O, Fe, C and W elements at the center of the worn scar of the C3 specimen after sliding at 50N 20Hz.	138
Figure 4.23:	(a) Stribeck curves for NC, C1 and C3 specimens and (b) Stribeck curves for M1 and M3 specimens.	144
Figure 4.24:	Stribeck curves at boundary and mixed lubrication where (a) Stribeck curves for C1 and C3 specimens and (b) Stribeck curves for M1 and M3 specimen	145
Figure 4.25:	SEM images of the NC specimen produced after sliding at (a) 10N (b) 50 N and (c) 150 N under oil lubrication. (d) and (e) are the enlargement of areas A and B in figure (c). The worn scar produced at 10 N was relatively smooth. 50 N load produced worn scar dominated by grooves. The center of the worn scar after sliding at 150 N showed evidence of tearing due to scuffing.	146
Figure 4.26:	Worn surface of the C3 specimen tested under lubrication condition at (a) 10 (b) 150 and (c) 400 N.	147
Figure 4.27:	SEM images of the C1 specimen produced after sliding at (a-b) 10N (c) 50 N and (d) 1000 N under oil lubrication.	148
Figure 4.28:	SEM images of the (a) grooved formed on the M1 specimen after sliding at 50N and (b) fracture surface formed on the M1 specimen after sliding at 600 N under oil lubrication.	148

Figure 4.29:	Effect of load on the volume loss under lubricated sliding for (a) NC, C1, C3, M1 and M3 specimens at 10-400N and (b) C1, C3, M1 and M3 specimens at 600-1000N. 600N(i) and 1000N(i) indicate that no fracture took place on the worn surface while 600N(ii) and 1000N(ii) indicated that fracture took place during sliding.	149
Figure 4.30:	The wear area of C1 material tested under lubrication condition of 10N20hz.	150
Figure 4.31:	The worn scar and the respective COF graph for M1 specimen subjected to lubrication test at (a) 400N 20Hz, (b) 600N 20Hz (fractured) and (c) 600N 20Hz (non fractured) (d) 1000N 20Hz (fractured) and (e) 1000N 20Hz (non fractured).	151
Figure 4.32:	The worn scar and the respective COF graph for M3 specimens subjected to lubrication test at (a) 400N 20Hz, (b) 600N 20Hz (fractured) and (c) 600N 20Hz (non fractured) (d) 1000N 20Hz (fractured) and (e) 1000N 20Hz (non fractured).	152
Figure 4.33:	The worn scar and the respective COF graph for C3 specimens subjected to lubrication test at (a) 400N 20Hz, (b) 600N 20Hz and (c) 1000N 20Hz.	153
Figure 4.34:	The worn scar and the respective COF graph for C1 specimens subjected to lubrication test at (a) 400N 20Hz, (b) 600N 20Hz and (c) 1000N 20Hz.	154
Figure 4.35:	The weight percentage of carbon and iron at the centre of the worn scar of the C1 specimens produced at different loads.	155
Figure 4.36:	The weight percentage of carbon and iron at the side of the worn scar of the C1 specimens produced at different loads.	155

Figure 4.37:	The weight percentage of oxygen, sulfur, zinc and phosphorus at the center of the worn scar of the C1 specimens produced at different loads.	155
Figure 4.38:	The weight percentage of oxygen, sulfur, zinc and phosphorus at the side of the worn scar of the C1 specimens produced at different loads.	156
Figure 4.39:	The weight percentage of carbon and iron at the worn scar of the NC specimens produced at different loads.	157
Figure 4.40:	The weight percentage of oxygen, sulfur, zinc and phosphorus at the worn scar of the NC specimens produced at different loads.	157
Figure 4.41:	The weight percentage of carbon and iron at the worn scar of the M1 specimens produced at different loads.	158
Figure 4.42:	The weight percentage of oxygen, sulfur, zinc and phosphorus at the worn scar of the M1 specimens produced at different loads.	158



## LIST OF ABBREVIATIONS

<b>ASTM</b>	- American society for testing and materials
<b>BCC</b>	- Body centred cubic
<b>BCT</b>	- Body centred tetragonal
<b>CCT</b>	- Continuous cooling transformation
<b>C1</b>	- 1 hour carburised
<b>C3</b>	- 3 hour carburised
<b>CO</b>	- Carbon monoxide
<b>CO<sub>2</sub></b>	- Carbon dioxide
<b>COF</b>	- Coefficient of friction
<b>DPH</b>	- Diamond pyramid hardness
<b>EDX/EDS</b>	- Energy-dispersive X-ray spectroscopy
<b>EHL</b>	- Elasto hydrodynamic
<b>FCC</b>	- Face centred cubic
<b>HD</b>	- Hydrodynamic
<b>HRC</b>	- Rockwell hardness
<b>HTTP</b>	- High temperature transformation product
<b>HV</b>	- Vickers hardness
<b>H<sub>2</sub>O</b>	- Water
<b>ICDD</b>	- International Centre for Diffraction Data
<b>IT</b>	- Isothermal transformation
<b>KCl</b>	- Potassium chloride
<b>LTCSS</b>	- Low temperature colossal supersaturation
<b>M1</b>	- 1 hour martensite
<b>M3</b>	- 3 hour martensite
<b>Na<sub>2</sub>CO<sub>3</sub></b>	- Sodium carbonate
<b>NaCl</b>	- Sodium chloride
<b>NC</b>	- Non carburised
<b>SEM</b>	- Scanning electron microscope
<b>XRD</b>	- X-ray diffraction
<b>ZDDP</b>	- Zinc-dialkyl-dithiophosphate

## LIST OF SYMBOLS

<b>%</b>	-	percentage
<b>+ve</b>	-	positive
<b>-ve</b>	-	negative
<b>A</b>	-	amphere
<b>C</b>	-	carbon
<b>Cr</b>	-	Chromium
<b>Cu</b>	-	Copper
<b>E</b>	-	electron
<b>Fe</b>	-	iron
<b>H</b>	-	height
<b>Hr</b>	-	hour
<b>In</b>	-	inches
<b>ml</b>	-	millilitre
<b>mm</b>	-	millimetr
<b>Mn</b>	-	Manganese
<b>Mo</b>	-	Molybdenum
$\eta$	-	viscosity
<b>N</b>	-	Newton
<b>Na</b>	-	Sodium
<b>Ni</b>	-	Nickel
<b>O</b>	-	Oxygen
<b>R<sub>a</sub></b>	-	Average roughness
<b>Si</b>	-	Silicone
<b>Ti</b>	-	Titanium
<b>V</b>	-	volt
<b>V</b>	-	Velocity
$\mu\text{m}$	-	micrometer
$^{\circ}$	-	degrees
$^{\circ}\text{C}$	-	Degrees celcius

## LIST OF EQUATIONS

		Page
Equation 1.1:	Case depth $\propto K\sqrt{\text{Time}}$	5
Equation 2.1:	$\frac{\partial C}{\partial t} = D \frac{\partial^2 C}{\partial x^2}$	13
Equation 2.2:	$\frac{C_x - C_0}{C_s - C_0} = 1 - \text{erf}\left(\frac{x}{2\sqrt{Dt}}\right)$	14
Equation 2.3:	$D = D_0 \exp\left(-\frac{Q_d}{RT}\right)$	17
Equation 2.4:	$M_s = 561 - 474C - 33Mn - 17Ni - 17Cr - 21Mo$	24
Equation 2.5:	$Na_2CO_3 = 2Na + CO_3^{2-}$	39
Equation 2.6:	$CO_2 + 4Na = 2Na_2O + C$	39
Equation 2.7:	$CO + 2Na = Na_2O + C$	39
Equation 2.8:	$CO_3^{2-} + Fe + 4e \Rightarrow C - Fe + 3O^{2-}$	39
Equation 2.9:	$CO_3 + 2C = 3CO$	39
Equation 2.10:	$CO_2 + C = 2CO$	39
Equation 2.11:	$2O^{2-} \Rightarrow O_2 + 4e$	39
Equation 2.12(a):	$O^{2-} + CO_2 \Rightarrow CO_3^{2-}$	40
Equation 2.12(b):	$CO_2 + Na_2O = Na_2CO_3$	40